Eur. J. Mineral.
2001, **13**, 485-495

This paper was presented at the EMPG VIII
meeting in Bergamo, Italy (April 2000)

Antigorite: Pressure and temperature dependence of polysomatism and water content

BERND WUNDER*, RICHARD WIRTH and MATTHIAS GOTTSCHALK
GeoForschungsZentrum Potsdam, Division 4.1, Telegrafenberg, D-14473 Potsdam, Germany

Abstract: The pressure and temperature dependence of antigorite polysomatism was investigated in the P,T-range of 350-710°C, 0.2-5.0 GPa within the system MgO-SiO_2-H_2O (MSH). TEM-study indicated that increasing temperature and decreasing pressure of MSH-antigorite formation are correlated with a shorter *a*-cell periodicity, *i.e.* smaller *m*-value (*m* = number of tetrahedra in a single chain along the wavelength *a*). For the P,T-conditions investigated, the compositional *m*-range of antigorite is rather narrow (14-18) corresponding to $Mg_{2.79}Si_2O_5(OH)_{3.57}$ – $Mg_{2.83}Si_2O_5(OH)_{3.67}$. The change in the crystal structure of antigorite is combined with a gradual partial dehydration process and loss of MgO.

For the formulation of reactions that include antigorite, the P,T-dependence of the chemical composition of antigorite has to be considered. However, our results support the conclusion of Mellini *et al.* (1987) of the limited applicability of a modulation-dependent geothermobarometer, because equilibrium states of antigorite modulation are rarely observed in natural occurrences and have not been reached in our experiments.

The successive partial dehydration of antigorite during ongoing subduction of serpentine-bearing oceanic lithosphere probably influences its rheological properties.

Key-words: antigorite, polysomatism, high-pressure experiments, serpentine, TEM.

Introduction

The serpentine variety antigorite, which is among the most hydrous rock-forming silicates known, is proposed to be the predominant phase for carrying large amounts of water into the upper mantle during subduction of hydrated ultrabasic rocks (*e.g.* Ulmer & Trommsdorff, 1995). Despite large differences in recent experimental results with respect to the breakdown of antigorite (Ulmer & Trommsdorff, 1995; Wunder & Schreyer, 1997; Bromiley & Pawley, 2000), these studies indicate that antigorite is the only serpentine mineral which is stable to depths at which arc magmas generate (90-150 km, *e.g.* Schmidt & Poli, 1998). Water-induced and influenced processes within subduction zones, like triggering of partial melts, metasomatic alteration or even seismicity (due to processes like dehydration embrittlement), are proposed to be strongly associated with the dehydration of antigorite within these regions.

Antigorite is not a polymorph of the other two rock-forming serpentine phases lizardite and chrysotile ($Mg_3Si_2O_5(OH)_4$) because it forms discrete compositions lying on the join between chrysotile and talc ($Mg_3Si_4O_{10}(OH)_2$) in the system MgO-SiO_2-H_2O (MSH, Fig. 1). The chemical difference between antigorite and the rolled-layered chrysotile and flat-layered lizardite is the result of its unique wavelike structure // the *a*-axis of antigorite (Fig. 2). At the planes of inversion of the sinusoidal tetrahedral and octahedral layers, which are characterized by a reversion of tetrahedral polarity within every half wavelength, the Mg

*E-mail: wunder@gfz-potsdam.de

DOI: 10.1127/0935-1221/2001/0013-0485 0935-1221/01/0013-0485 $ 2.75

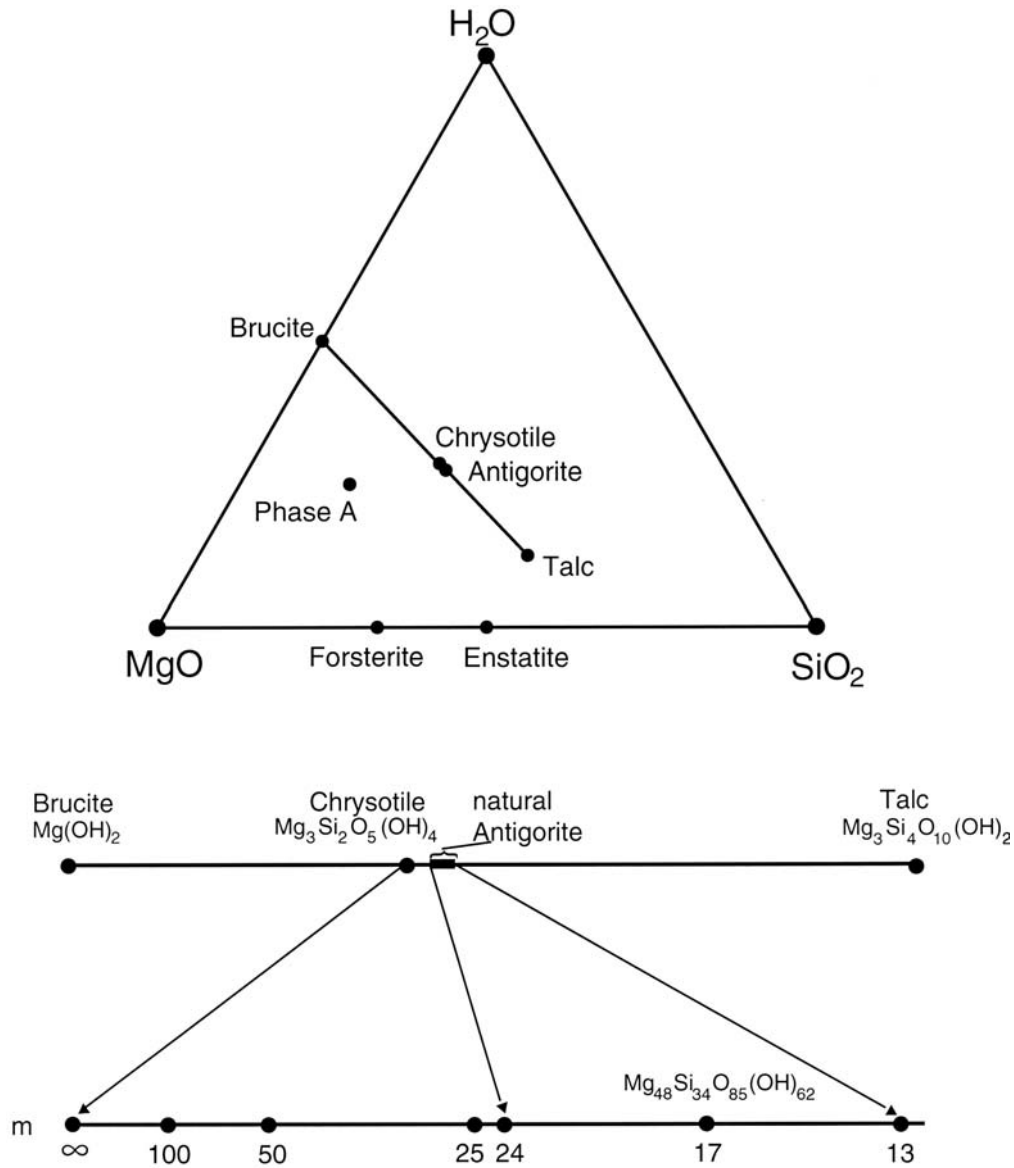

Fig. 1. Selected phases of the system MgO-SiO_2-H_2O (MSH) and enlarged projection of the tie-line brucite – talc with the range of chemical variations of natural antigorites according to Mellini *et al.* (1987), defined by *m*-values (see text).

and OH content is reduced relative to Si. Therefore, the water and Mg content of antigorite increases and the Si content decreases with increasing wavelength *a*. According to Kunze (1961), compositional variations of antigorite can be expressed by the formula $M_{3m-3}T_{2m}O_{5m}(OH)_{4m-6}$ (M = octahedral cations like Mg , Fe^{2+}, Ni, Al; T = tetrahedral cations like Si, Al, Fe^{3+}; *m* = number of tetrahedra in a single chain along the wavelength *a*). Chapman & Zussman (1959) observed *a* cell dimensions between 16.8 and 109 Å, which would correspond to *m*-values of 7 to 41. However, Mellini & Zussman (1986) discovered that "antigorites" of very low *a*-values between 16.8 and 33.7 Å were misidentifications of carlosturanite, which has the ideal formula $Mg_{42}Si_{24}O_{56}(OH)_{68}(H_2O)_2$.

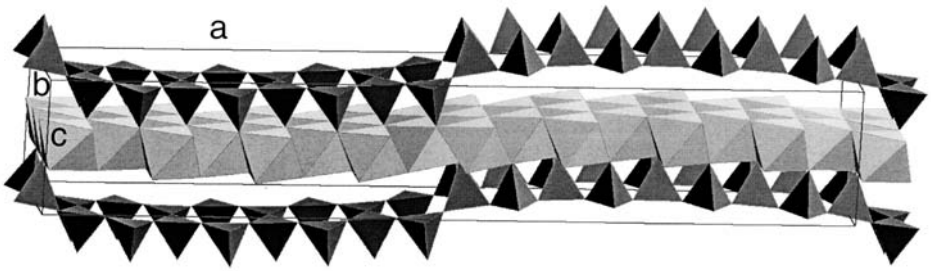

Fig. 2. Crystal structure of antigorite with m = 17. Structural data for this drawing are taken from Uehara (1998).

Therefore, these authors suggested a lower *a*-limit of about 33 Å (m = 13) for antigorite. Assuming a pure MSH-composition, the water content of antigorites with m = 13-41 is in the range 12.09-12.72 wt.%. According to Mellini *et al.* (1987), typical compositions of natural antigorites (Fig. 1) are in the limited *m*-range of 13-24, which would correspond to a water content of 12.09-12.52 wt.%. Their TEM-study indicated a T-dependence of the *m*-value. With increasing metamorphic grade of the serpentinite they observed a decrease of the *m*-values. The same inverse relation between the *m*-value and metamorphic grade was already predicted in former studies by Kunze (1961) and Trommsdorff (1983) and later again verified by Uehara & Kamata (1994). Mellini *et al.* (1987) proposed that a *m*-value dependent geothermometer might have limited applicability, because most of the natural antigorite samples investigated by TEM showed a heterogeneous distribution of *m*-values even in one antigorite grain.

No systematical experimental studies of the P, T-dependence of the *m*-value, *i.e.* water content and MgO-loss, of antigorite have yet been performed. Knowledge of the poorly defined structural state and chemistry of antigorite at high pressures and temperatures is urgently required for a better understanding of the geological processes mentioned above. Therefore, the aim of this experimental study was to investigate antigorite polysomatism over a wide range of P and T for samples synthesized in the pure Al- and Fe-free MSH-system, and to test if antigorite can be used as a possible geothermobarometer.

Experimental methods

Synthesis experiments up to 0.5 GPa were performed in standard cold-seal hydrothermal pressure vessels and high-pressure runs up to 4.0 GPa in an end-loaded piston-cylinder apparatus at the

Table 1. Results of experiments bearing on the synthesis of antigorite.

Run No.	P[GPa]	T[°C]	t[d]	solid run products
287	5.0	500	7	Ant*, Chr*(tr), Br(tr)
476/1	4.0	500	14	Ant*, Chr*(tr), Br
477/2	3.5	600	4	Ant*, Chr*(tr), Fo
484/2	2.0	450	14	Ant*, Chr*, Fo
488	1.5	600	21	Ant*, Chr*(tr), Fo
490	0.5	500	35	Ant*(tr), Chr*, Fo
491	0.2	450	35	Chr*, Fo
494	3.5	600	14	Ant*, Chr*(tr), Fo
499/1	1.5	500	21	Ant*, Chr*, Fo
505/1	2.1	710	28	Tc, Fo
507	1.0	350	22	Tc, Br, Fo, Ant*, Chr*

*determined by TEM
Abbreviations: Ant: antigorite; Chr: chrysotile; Fo: forsterite; Br: brucite; Tc: talc; (tr): traces.

GeoForschungsZentrum Potsdam. An additional experiment (no. 287, Table 1) at 5.0 GPa was performed at the University of Bochum. This experiment has been described in detail by Wunder *et al.* (1997). Temperatures within the hydrothermal autoclaves were recorded by NiCr/Ni thermocouples, which were closely adjoined to the samples. Pressure was controlled with a calibrated strain gauge. Estimated uncertainties for the temperature are less than ± 5°C and for the pressure ± 10 MPa. In each piston-cylinder run, up to two Au-tubes of about 10 mm length and 2 mm in diameter were positioned in NaCl-steel assemblies of 1.28 cm in diameter (see also Massonne & Schreyer (1986), their Fig. 2, pressure-cell type I). The temperature was monitored using a chromel-alumel thermocouple, and was controlled within ± 2°C during the experiment. No pressure correction was made for the measured potential differences of the thermocouple. The piston-cylinder apparatus was calibrated using the α-quartz/coesite transition after Mirwald & Massonne (1980). The 2σ-uncertainties in pressure and temperature were approximately ± 2 % and ± 10°C, respectively. For solid starting materials brucite and talc synthesized as pure MSH-phases (Wunder *et al.,* 1997) were used. Except for run 287, brucite and talc were mixed in the stoichiometric proportions corresponding to an antigorite with a *m*-value of 17 ($Mg_{48}Si_{34}O_{85}(OH)_{62}$, Fig. 1). 20 wt.% of water was added to 10 mg of crystalline starting material. Run-durations varied between 4 and 35 days. The antigorite composition mentioned above is often chosen as a typical one for antigorite in the literature (*e.g.* Berman, 1988). In the following, with the exception of reactions summarized in Table 2 (see later), antigorite formulae will be presented on the basis of two silicon atoms, to give an immediate idea of the compositional change with increasing or decreasing structural modulation.

Powder XRD patterns of the run products were recorded in the 2θ-range of 5-125° (Cu$K\alpha_1$-radiation) using a fully automated STOE STADI P diffractometer. TEM investigations were carried out with a Philips CM200 transmission electron microscope equipped with an EDAX X-ray analyser and a Gatan image filtering system GIF. The microscope was operated at 200 kV with a LaB_6 cathode as electron source. A double-tilt specimen holder with Be specimen cradle was used to achieve suitable orientations for lattice fringe imaging. All images are energy filtered, by applying a 10 eV window to the zero-loss beam. The problem of irradiation damage was effectively reduced by using the CCD camera of the GIF to achieve an exposure time of under 1 s. An indicated magnification of the microscope of 6600 was used. The additional magnification due to the CCD camera (of the GIF) resulted in a total magnification of 118000. At this magnification, the specimen can be investigated under defocused beam conditions, thus further reducing beam damage. The wave-like structure of antigorite is only visible in a [010] oriented foil that reveals the *a* and *c* lattice parameters. However, antigorite has a very pronounced cleavage parallel to (001). This excludes powder preparation by sedimentation of the dispersed powder onto a copper grid covered with a holey carbon film. For that reason we used a technique that made it more likely to obtain the favourable [010] orientation of antigorite grains, which, in principle, has already been described by Amouric *et al*. (1981) for synthetic mica, and is therefore only briefly documented herein. A rectangular hole ($2 \cdot 2$ mm^2) was cut into a 100 µm thick adhesive tape. The tape was fixed to a glass plate and the resulting volume ($2 \cdot 2 \cdot 0.1$ mm^3) was filled with a mixture of epoxy and antigorite and then covered by a glass, hardened, and cut in two pieces. The halves were rotated by 90 degrees, again embedded in epoxy, and a normal thin section of the specimen was prepared. The majority of the (001) planes of antigorite were now oriented normal to the surface of the thin section. The specimen preparation was continued by conventional ion-beam thinning until electron transparency was achieved, and finally coated with a thin carbon film to prevent charging in the TEM.

Results

The experimental conditions of the syntheses are summarized in Table 1. XRD analysis revealed that in all but one experiment serpentine had formed. However, from the X-ray powder diffraction no distinct identification of the variety of serpentine formed could be obtained. In addition to serpentine, brucite, forsterite and talc were produced. According to Peacock (1987), antigorite exhibits a characteristic X-ray reflection at a d-value of 1.53 Å, which is not present for chrysotile and lizardite. However, this could not be used for a reliable identification of antigorite, because reflections of the other phases overlap with the weak 1.53 Å reflection of antigorite. X-ray powder diffraction reflections of serpentine are very broad. TEM-investigations (see below) indicate that the broadness of reflections is a combined effect of the occurrence of mixtures of different

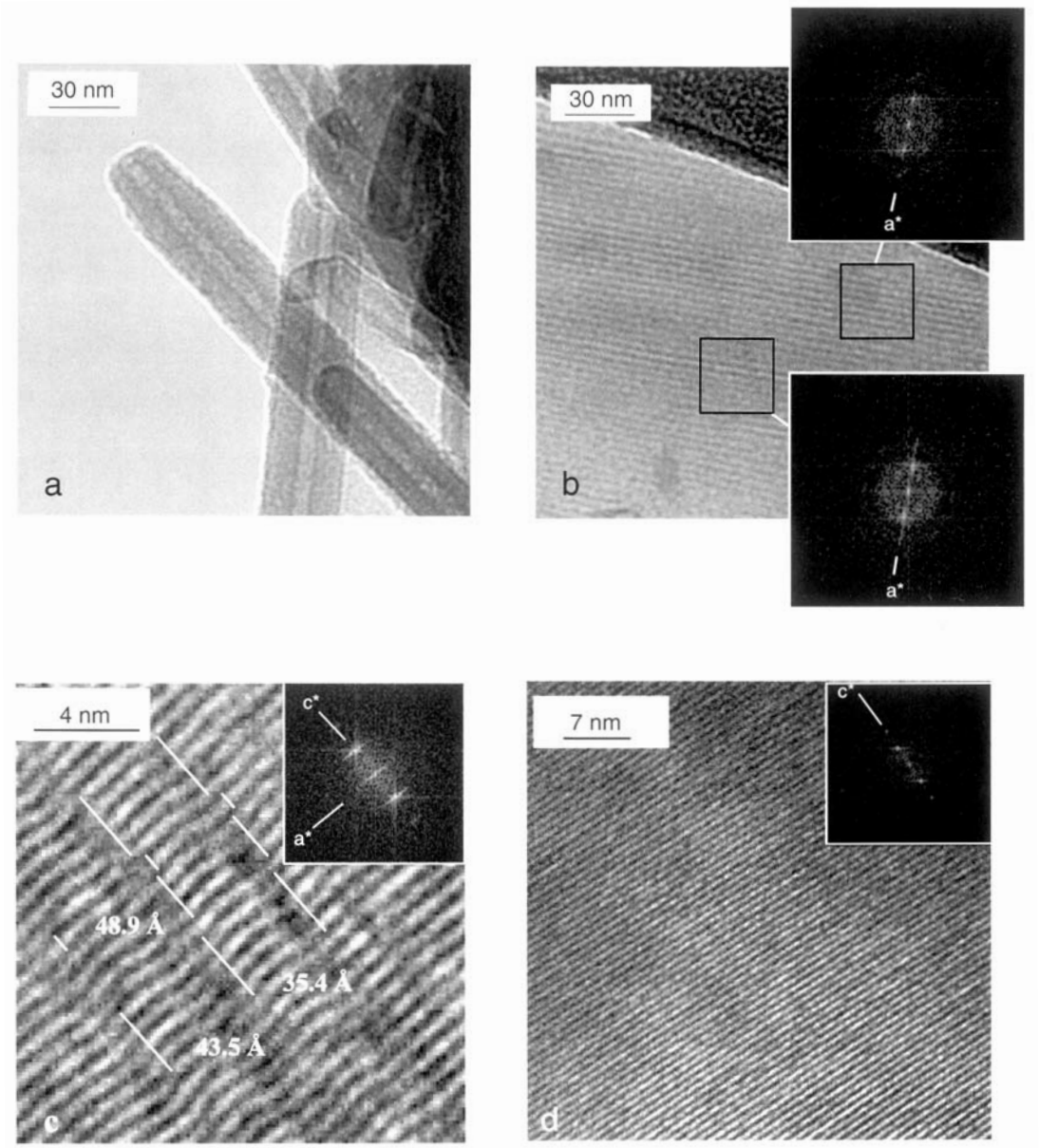

Fig. 3. (a) TEM-image of chrysotile (# 490), (b) TEM-image of (100) lattice fringes of antigorite (# 488), (c) HRTEM-image of antigorite (# 488) showing characteristic wavy layers, (d) TEM-image of (001) lattice fringes of antigorite (# 488).

structural states of antigorite, of different serpentine varieties, and the very small grain size of serpentine crystals. Therefore, no structure determination using the Rietveld method could be obtained. The occurrence in run 507 (Table 1) of brucite plus talc, used as the solid starting material, indicates an incomplete reaction at the low temperature of 350°C after 22 days.

Differences in the composition of antigorite are difficult to determine by electron microprobe (EMP) because they are rather small and lie within the analytical error of EMP measurements.

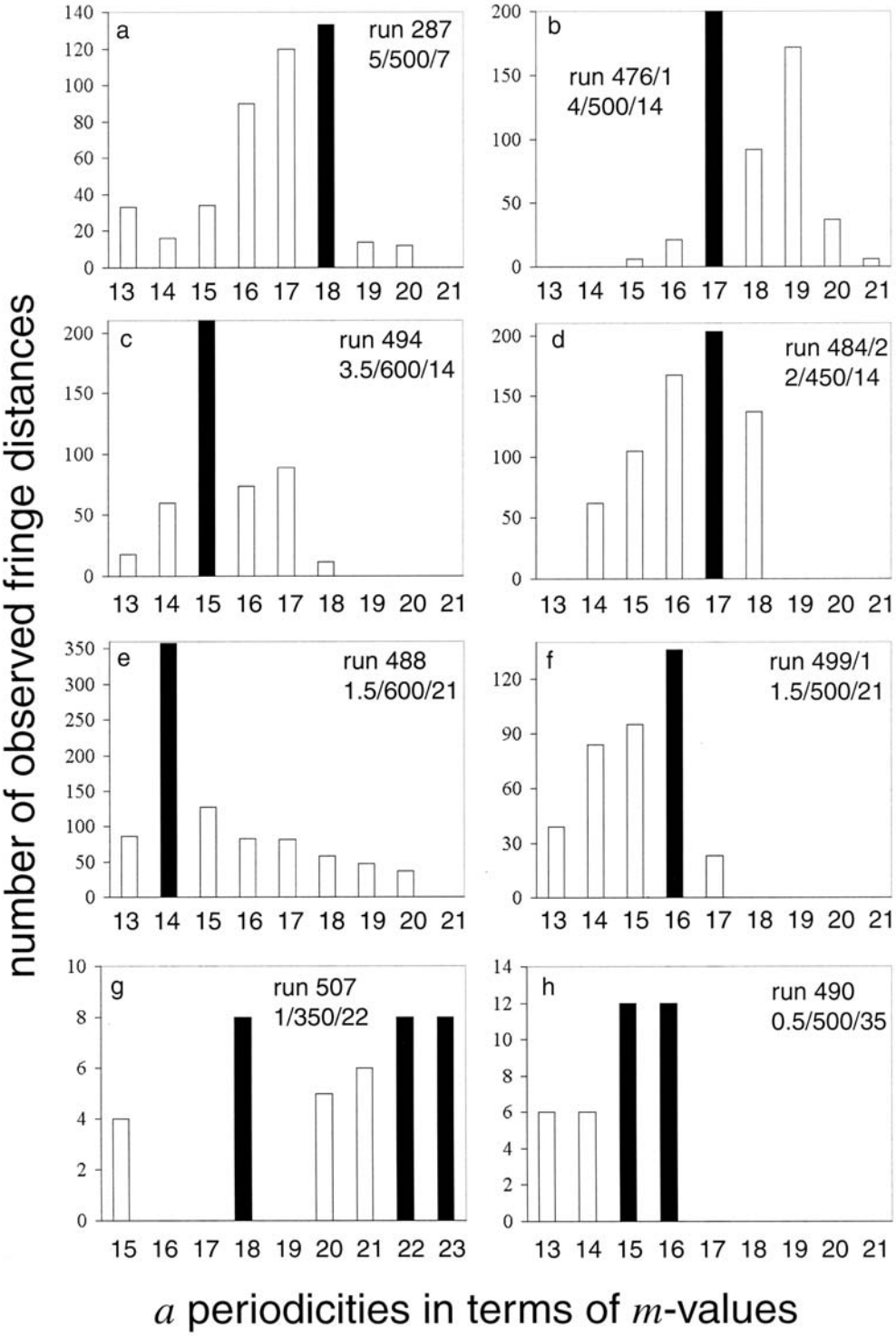

Fig. 4a-h. Periodicity distribution of synthetic antigorites (see Table 1). P[GPa]/T[°C]/t[d]. Filled symbols: most frequent *a* periodicities.

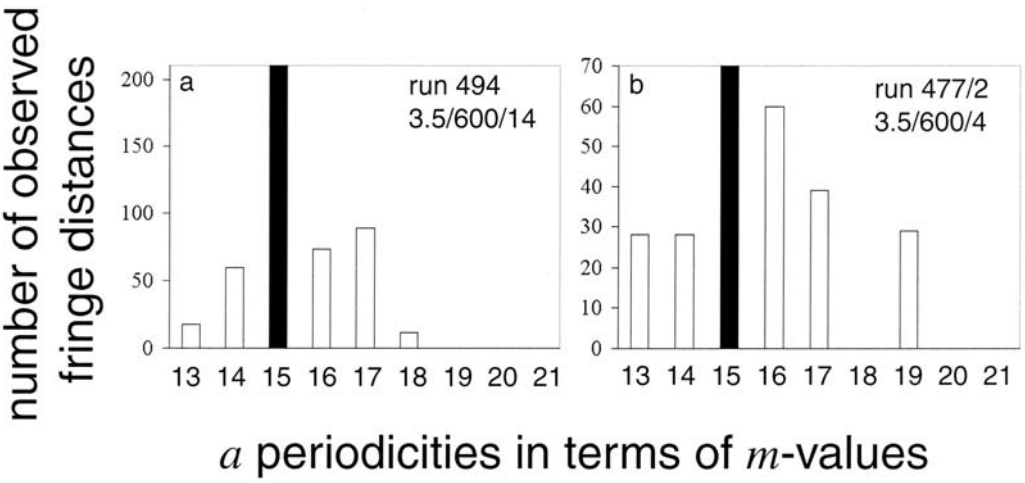

Fig. 5a, b. Antigorite periodicity distributions for two samples obtained at the same P,T-conditions but for different run-durations. Symbols are the same as in Fig. 4a-h.

Additionally, as the grain size of synthesized antigorites (Ø < 0.3 μm) was not large enough for reliable EMP-measurements, compositions and structure were instead determined by transmission electron microscopy (TEM) by measuring the *a* cell dimensions of the synthetic MSH-antigorite. The *a* lattice modulation and therefore the corresponding *m*-value was determined from lattice fringe images as follows: After acquiring the energy-filtered lattice-fringe image, a representative area (5-30 fringes) of an antigorite crystal was selected to calculate a fast Fourier transform (FFT) resulting in a diffraction pattern of the selected area. The d-spacing of the *a* lattice fringes was determined from the calculated diffraction pattern, which gives an average of the reciprocal lattice of the selected area. This method was performed for several antigorite grains in each sample. For the determination of the *m*-value distribution (see later), the amount of fringes within each of the selected areas was counted. Only regions of lattice fringes with a single *m*-value were used. A FFT of such a region showed sharp reflections (upper selected area of Fig. 3b), whereas for regions with varying lattice fringe distances smeared or split reflections (lower selected area of Fig. 3b and Fig. 3c) were observed.

The TEM-investigation indicated that in all but one run containing serpentine (Table 1) a mixture of the two serpentine phases, antigorite and chrysotile, had formed during the experiment. Lizardite was not observed in any of the run products. Due to their different lattice fringe images, *a* cell dimensions and morphology, chrysotile and antigorite could clearly be distinguished by TEM: chrysotile forms rolls with hollow cores (Fig. 3a); antigorite forms anhedral very thin (< 150 nm) flakes (Fig. 3b). As roughly estimated by our TEM study, the amount of antigorite within the samples seems to increase with increasing temperature and pressure of the experiments. In all runs above 1.5 GPa only traces of chrysotile could be observed. At low pressures and temperatures such as 0.2 GPa, 450°C, chrysotile was the only serpentine phase that formed.

Antigorites show a heterogeneous distribution of periodicities even in one grain. Measured *m*-values are in the range 13-23. This range is in agreement with the *m*-value range observed by Mellini *et al*. (1987) for natural samples. For the determination of the periodicity distribution (Fig. 4a-h, 5a,b), TEM-measurements were performed over several grains. For samples 490 and 507, only a few antigorite fringe widths were measured. Therefore, these periodicity distributions have to be treated with caution. The most frequent value of *m* determined within each sample (Fig. 4a-h) seems to be a function of P and T. With increasing temperature and decreasing pressure the most frequent *m*-value (water- and MgO-content) of antigorite decreases.

As already observed for natural antigorite (Otten, 1993), synthetic antigorite is extremely sensitive to beam damage. Therefore, details of the wavelike structure of antigorite (Fig. 3c) were only visible in high-resolution images along its [010] zone axis in very thin flakes (< 15 nm) using the procedure described above to avoid beam

damage. For such orientations satellite reflections aligned along *a** are visible (Fig. 3c). These are characteristic for the periodic lattice modulation of antigorite. The satellite reflections are smeared along *a** due to the occurrence of varying modulation lengths. Such regions were not taken for determination of the *a*-periodicity distribution (see above). Additionally, disordering of layer stacking is visible (Fig. 3c). Such offsets of layers along *a* have already been described for natural antigorite (*e.g.* Otten, 1993). According to Spinnler (1985) the magnitude of displacement should amount x · 2.7 Å. Contrary to the variation in *a*-cell dimensions, lattice fringe distances observed for (001) layers of the synthetic antigorite are rather homogeneous, with spacings of about 7.25 Å (Fig. 3d).

Discussion

In our experimental study, we found that an increasing temperature, and less distinctly, a decreasing pressure of MSH-antigorite formation can be correlated with a shorter *a*-cell periodicity of antigorite. This is in accordance with Mellini *et al.* (1987), who described the same temperature effect for natural antigorite samples. As shown in Fig. 6, the *m*-value (17) of the natural antigorite sample Mg 159 (Mellini *et al.*, 1987) is consistent with the experimentally determined most frequent *m*-values. The natural sample Mg 159 was chosen for comparison, because it is structurally (Mellini *et al.*, 1987) and chemically (Ulmer & Trommsdorff, 1995) extensively characterized. Additionally, its P,T-conditions of formation are rather well known: according to Mellini *et al.* (1987) and Mellini (pers. comm., 2000) temperatures of 435 (± 30) °C and low pressures less than 0.2-0.3 GPa were estimated for Mg 159. From our knowledge, this natural antigorite is the only one described in the literature that has a single *m*-value (17). Uehara (1998) investigated the structural modulation of natural antigorite coming from a suite of well constrained metamorphic settings

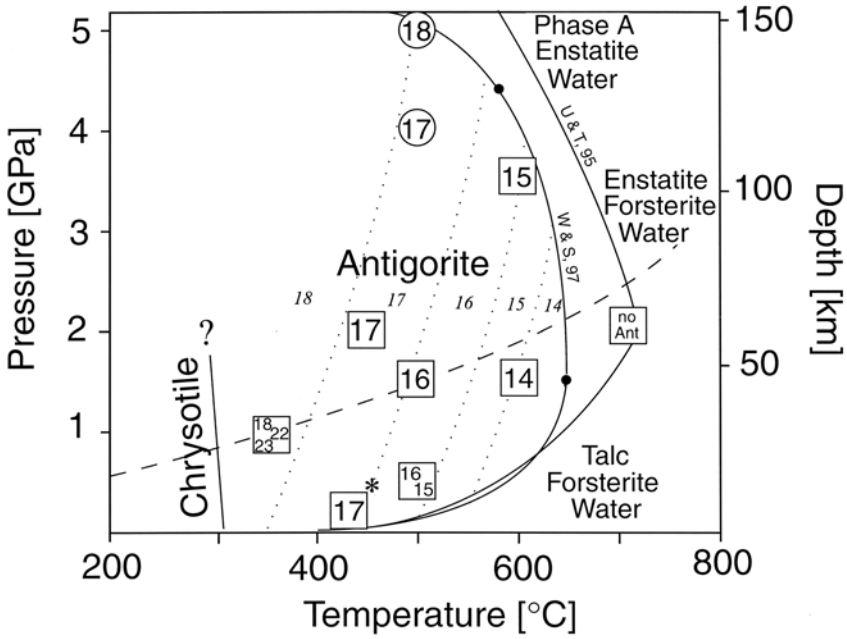

Fig. 6. P,T-dependence of the most frequent *m*-values as determined from the periodicity distribution (Fig. 4a-h and 5) of synthetic antigorite from different parageneses (forsterite + antigorite: squared numbers; brucite + antigorite: circled numbers). Based on these data, dotted lines limit P,T-ranges for different *m*-values (labelled by italic numbers), which decline according to reaction (5, see text). * indicates the *m*-value of a natural antigorite as determined by Mellini *et al*. (1987). Maximum stability fields of antigorite are shown as determined experimentally by Ulmer & Trommsdorff (1995) (U & T, 95) and Wunder & Schreyer (1997) (W & S, 97). The chrysotile to antigorite transformation is taken from Evans *et al.* (1967). The dashed line represents a theoretical P,T, t-path for the subduction of a 50 Ma old oceanic crust as modelled by Peacock (1990). Abbreviations: Ant, antigorite; Br, brucite; Fo, forsterite; A, phase A; W, water.

ranging from low- to high-grade metamorphic conditions. All these samples showed a heterogeneous distribution of periodicities (the overall range of variations extends from 28 to 61 Å), and, contrary to Mellini *et al.* (1987) and the results presented within this study, no significant relation of these values to the temperature of antigorite formation was obvious.

Equilibrium and antigorite stability

To test whether we had determined the "stable" antigorite configurations, we performed two runs (no. 477/2, no. 494, Table 1, Fig. 5a,b) at the same P,T-conditions but at different run-durations. The same most frequent *m*-value (15) was determined for both runs, but with increasing run duration the *m*-value distribution became sharper (Fig. 5a,b).

Both the varying *a*-cell periodicities of antigorite and the additional serpentine phase chrysotile, which was observed in all of our experiments up to temperatures of 600°C (Table 1), indicate that we have not reached equilibrium conditions within our experiments. The breakdown of chrysotile to antigorite plus brucite occurs at about 310°C (at 1 bar) and the reaction is shifted to lower temperatures for higher pressures (Evans *et al.*, 1976, see Fig. 6). The extreme sluggishness of the chrysotile to antigorite transformation is known from natural occurrences as well as from experimental studies (Evans *et al*., 1976). Very small energetic differences between antigorites of different periodicities and slow kinetics or quench problems, might account for the formation of varying *m*-values, which have been observed in all of our synthetic samples. With the exception of only one known natural occurrence (sample Mg 159, see above), mixtures of different periodicities, even within one grain, are also common in natural antigorite. According to Viti & Mellini (1996), who investigated the modulation periodicity of vein antigorite, the sluggish chrysotile – antigorite transformation as well as the polysomatic equilibrium of antigorite will be accelerated by deformation processes and/or an abundant fluid phase.

Assuming that the most frequent *m*-values of measured periodicity distributions (Fig. 4) represent the stable configurations at P and T (with the exception of run 507), MSH-antigorite seems to have stable *m*-values only within the very narrow limits of 14 to 18, corresponding to the compositional range $Mg_{2.79}Si_2O_5(OH)_{3.57}$ – $Mg_{2.83}Si_2O_5(OH)_{3.67}$. The difference in the water content of these two antigorite members is only 0.19 wt.%. One might assume that for higher pressures and lower temperatures than the P,T-conditions chosen in this study, antigorite with larger *m*-values than 18 might occur. However, such extremely high P/T-conditions seem not to be the case within the mantle or the crust.

The *m*-value of antigorite is not only dependent on P and T but also on additional factors: *e.g.* (1) the parageneses within which antigorite formed, (2) the water activity during antigorite formation, (3) composition of antigorite (especially its aluminium and iron content). Within our experiments we observed forsterite together with antigorite at $P \leq 3.5$ GPa and brucite plus antigorite at higher pressures (see Fig. 6). Phase A was not observed within our experiments. Therefore, these results give additional information on the P,T-dependence of the antigorite *m*-values of the two parageneses. However, it is completly unknown how or to what extent other parageneses (*e.g.* with phase A or chlorite for Al-containing compositions) will influence the modulation of antigorite. As long as these uncertainties are not clarified, our results strengthen the conclusion of Mellini *et al.* (1987) of the limited applicability of a *m*-value dependent geothermobarometer.

Recently, Bromiley & Pawley (2000) showed that even small amounts of aluminium can increase the antigorite stability field to higher temperatures. Indirectly this was supported by run no. 505/1 (Table 1). Run no. 505/1, which was performed at P,T-conditions within the stability of an Al-rich antigorite according to Ulmer & Trommsdorff (1995), but outside the P,T-limits given by Wunder & Schreyer (1997) for an Al-poor and/or Al-free antigorite, gave no antigorite but the solid breakdown assemblage talc plus forsterite (see Fig. 6). Perhaps smaller *m*-values than the minimum value of 14 observed within this study can be stabilized for Al-rich antigorite at temperatures exceeding the stability of MSH-antigorite.

Antigorite reactions

With various internally consistent thermodynamic datasets (*e.g.* Berman, 1988; Gottschalk, 1997; Holland & Powell, 1998) equilibrium calculations are performed using a fixed antigorite composition of $m = 17$. However, for any formulation of reactions that involve antigorite, the P,T-dependence of the *m*-value (and chemical composition) of antigorite has to be considered. For the simplest possible system MSH, antigorite formation or

Table 2. Summary of reactions (see discussion).

(1)	$18\ Mg_3Si_2O_5(OH)_4 <-> Mg_{51}Si_{36}O_{90}(OH)_{66}\ (m = 18) + 3\ Mg(OH)_2$
(2)	$5\ Mg_{39}Si_{28}O_{70}(OH)_{50}\ (m = 14) <-> 72\ Mg_2SiO_4 + 17\ Mg_3Si_4O_{10}(OH)_2 + 108\ H_2O$
(3a)	$Mg_{39}Si_{28}O_{70}(OH)_{50}\ (m = 14) <-> 11\ Mg_2SiO_4 + 17\ MgSiO_3 + 25\ H_2O$
(3b)	$Mg_{42}Si_{30}O_{75}(OH)_{54}\ (m = 15) <-> 12\ Mg_2SiO_4 + 18\ MgSiO_3 + 27\ H_2O$
(3c)	$Mg_{45}Si_{32}O_{80}(OH)_{58}\ (m = 16) <-> 13\ Mg_2SiO_4 + 19\ MgSiO_3 + 29\ H_2O$
(4a)	$5\ Mg_{45}Si_{32}O_{80}(OH)_{58}\ (m = 16) <-> 13\ Mg_7Si_2O_8(OH)_6 + 134\ MgSiO_3 + 106\ H_2O$
(4b)	$5\ Mg_{48}Si_{34}O_{85}(OH)_{62}\ (m = 17) <-> 14\ Mg_7Si_2O_8(OH)_6 + 142\ MgSiO_3 + 113\ H_2O$
(4c)	$Mg_{51}Si_{36}O_{90}(OH)_{66}\ (m = 18) <-> 3\ Mg_7Si_2O_8(OH)_6 + 30\ MgSiO_3 + 24\ H_2O$

breakdown corresponds to the reaction formalisms summarized in Table 2. Even if the experiment 507 (Table 1) does not give a clear result, we propose that the stable MSH-antigorite, that is formed together with brucite from chrysotile at low temperatures might have a *m*-value of 18. Therefore, within the pure MSH-system, the chrysotile breakdown should follow the water-conserving reaction (1, Table 2). At the highest temperatures (~ 650°C, at 1.5 GPa) of the MSH-antigorite stability as determined by Wunder & Schreyer (1997, Fig. 6), antigorite of $m = 14$ is stable. At pressures below 1.5 GPa antigorite with a *m*-value of 14 breaks down to form forsterite + talc + water according to reaction (2). Above 1.5 GPa antigorite with a *m*-value of 14 completely dehydrates to form forsterite, enstatite plus water according to reaction (3a), and towards higher pressures, as a result of the *m*-value transformations $14 \rightarrow 15 \rightarrow 16$, according to the reactions (3b) and (3c). At pressures above about 4.5 GPa antigorite breakdown (with $m = 16, 17, 18$) to phase A, clinoenstatite and water might follow the reactions (4a-c). In general, antigorites of adjacent periodicities in the presence of forsterite or brucite are related by the following two *m*-value transformation reactions:

$$(3 + m)\ \text{Antigorite}_{m+1} \leftrightarrow (4 + m)\ \text{Antigorite}_m + 6\ Mg_2SiO_4 + 9\ H_2O \quad (5),$$

$$m\ \text{Antigorite}_{m+1} \leftrightarrow (1 + m)\ \text{Antigorite}_m + 3\ Mg(OH)_2 \quad (6).$$

The decrease in *m* as a result of reaction (5) is schematically shown in Fig. 6. This diagram was drawn for a bulk composition between forsterite and antigorite, neglecting the phase brucite; the change of *m* according to the water-conserving reaction (6) is not shown. Thermodynamic calculations based on the internally consistent thermodynamic data of Gottschalk (1997) and a model of the Gibbs free energies for antigorites of different *m*-values will be presented elsewhere (Gottschalk & Wunder, in prep.).

Geodynamic implications

Within a subducting slab (Fig. 6), the first antigorite formed *via* reaction (1, Table 2) should have a *m*-value of 18. With increasing pressure and temperature antigorite runs through a structural and compositional evolution: the water content (and *m*-value) decreases continuously according to reaction (5) at P,T-conditions above (forsterite + water)-forming reactions. Therefore, according to reaction (5), subsequent small amounts of water will be produced and the amount of forsterite increases during an ongoing subduction process with depth. The amount of water which is set free during each of the four steps of *m*-reduction from 18 to 14 is rather small (each of them about 0.05 wt.%). This small amount of fluid might migrate into pores and might reduce the effective confining pressure thus leading to embrittlement (Raleigh & Paterson, 1965). Migration along interfaces might also change the adhesion of the grains. For example, from deformation experiments with labradorite it is known that thin melt films along interfaces (melt fraction of about 1 vol. %) will enhance the strain rate by about half an order of magnitude at constant stress (Dimanov *et al.*, 1998). Dehydration experiments of serpentinite under conditions of controlled pore water pressure revealed a weakening of the material with increasing temperature (Raleigh & Paterson, 1965). This was associated with sliding

in narrow shear zones containing ultrafine-grained olivine (Rutter & Brodie, 1988). Fine-grained olivine will also be produced by reaction (5) with increasing temperature.

As a consequence, for a better understanding of rheological processes such as dehydration embrittlement, which is supposed to be strongly associated with serpentinite dehydration and which is thought to be a possible explanation for seismicity within subduction zones, the progressive dehydration process of antigorite, described within this study, has to be considered.

Acknowledgements: The authors are grateful to E.-M. Schemmert, K. Paech and I. Bauer for sample preparation. The final version of the paper benefited from constructive reviews by B. W. Evans and M. Mellini and from comments of the associate editor D. Lattard.

References

Amouric, M., Mercuriot, G., Baronnet, A. (1981): On computed and observed HRTEM images of perfect mica polytypes. *Bull. Minéral.*, **104**, 298-313.

Berman, R.G. (1988): Internally consistent thermodynamic data for minerals in the system Na_2O-K_2O-CaO-MgO-FeO-Fe_2O_3-Al_2O_3-SiO_2-TiO_2-H_2O-CO_2. *J. Petrol.*, **29**, 445-522.

Bromiley, G.D. & Pawley, A.R. (2000): High pressure stability of antigorite in the systems MgO-SiO_2-H_2O and MgO-Al_2O_3-SiO_2-H_2O. *J. Conf. Abs.*, **5**, 17.

Chapman, J.A. & Zussman, J. (1959): Further electron-optical observations with crystals of antigorite. *Acta Cryst.*, **11**, 550-552.

Dimanov, A., Dresen, G., Wirth, R. (1998): Creep behaviour of partially molten polycrystalline labradorite. *Terra Nova Abstr. Supp.,* **1**, 12.

Evans, B.W., Johannes, W., Otterdoom, H., Trommsdorff, V. (1976): Stability of chrysotile and antigorite in the serpentine multisystem. *Schweiz. Mineral. Petrogr. Mitt.*, **56**, 79-93.

Gottschalk, M. (1997): Internally consistent thermodynamic data for rock forming minerals in the system SiO_2-TiO_2-Al_2O_3-Fe_2O_3-CaO-MgO-FeO-K_2O-Na_2O-H_2O-CO_2. *Eur. J. Mineral.*, **9**, 175-223.

Holland, T.J.B. & Powell, R. (1998): An internally consistent thermodynamic dataset for phases of petrological interest. *J. metamorphic Geol.*, **16**, 309-343.

Kunze, G. (1961): Antigorit. Strukturtheoretische Grundlagen und ihre praktische Bedeutung für die weitere Serpentin-Forschung. *Fortschr. Mineral.*, **39**, 206-324.

Massonne, H.-J. & Schreyer, W. (1986): High-pressure syntheses and X-ray properties of white micas in the system K_2O-MgO-Al_2O_3-SiO_2-H_2O. *N. Jb. Mineral. Abh.*, **153**, 177-215.

Mellini, M. & Zussman, J. (1986): Carlosturanite (not picrolite) from Taberg, Sweden. *Mineral. Mag.*, **50**, 675-679.

Mellini, M., Trommsdorff, V., Compagnoni, R. (1987): Antigorite polysomatism: behaviour during progressive metamorphism. *Contrib. Mineral. Petrol.*, **97**, 147-155.

Mirwald, P.W. & Massonne, H.J. (1980): Quartz — coesite transition and the comparative friction measurements in piston-cylinder apparatus using talc-alsimag-glass (TAG) and NaCl high pressure cells: A discussion. *N. Jb. Mineral. Mh.*, **1980**, 469-477.

Otten, M.T. (1993): High-resolution transmission electron microscopy of polysomatism and stacking defects in antigorite. *Am. Mineral.*, **78**, 75-84.

Peacock, S.M. (1987): Serpentinization and infiltration metasomatism in the Trinity peridotite, Klamath province, northern California: implications for subduction zones. *Contrib. Mineral. Petrol.*, **95**, 55-70.

— (1990): Fluid processes in subduction zones. *Science*, **248**, 329-337.

Raleigh, C.B. & Paterson, M.S. (1965): Experimental deformation of serpentinite and its tectonic implications. *J. Geophys. Res.*, **70**, 3965-3985.

Rutter, E.H. & Brodie, K.H. (1988): Experimental "syntectonic" dehydration of serpentinite under conditions of controlled pore water pressure. *J. Geophys. Res.*, **93**, B5, 4907-4932.

Schmidt, M.W. & Poli, S. (1998): Experimentally based water budgets for dehydrating slabs and consequences for arc magma generation. *Earth Planet. Sci. Lett.*, **163**, 361-379.

Spinnler, G.E. (1985): HRTEM study of antigorite, pyroxene-serpentine reactions and chlorite. Ph. D. thesis, Arizona State University, Tempe, Arizona, 248 p.

Trommsdorff, V. (1983): Metamorphose magnesiumreicher Gesteine: kritischer Vergleich von Natur, Experiment und thermodynamischer Datenbasis. *Fortschr. Mineral.*, **61**(2), 283-308.

Uehara, S. (1998): TEM and XRD study of antigorite superstructures. *Can. Mineral.*, **36**, 1595-1605.

Uehara, S. & Kamata, K. (1994): Antigorite with a large supercell from Saganoseki, Oita Prefecture, Japan. *Can. Mineral.*, **32**, 93-103.

Ulmer, P. & Trommsdorff, V. (1995): Serpentine stability to mantle depths and subduction-related magmatism. *Science*, **268**, 858-861.

Viti, C. & Mellini, M. (1996): Vein antigorites from Elba Island, Italy. *Eur. J. Mineral.*, **8**, 423-434.

Wunder, B. & Schreyer, W. (1997): Antigorite: High-pressure stability in the system MgO-SiO_2-H_2O (MSH). *Lithos*, **41**, 213-227.

Wunder, B., Baronnet, A., Schreyer, W. (1997): Ab-initio synthesis and TEM confirmation of antigorite in the system MgO-SiO_2-H_2O. *Am. Mineral.*, **82**, 760-764.

Received 19 October 2000
Modified version received 8 January 2001
Accepted 12 January 2001